Femtosecond Pump−Probe Spectroscopy of the B850 Antenna Complex of *Rhodobacter sphaeroides* at Room Temperature

V. Nagarajan,*,† E. T. Johnson,† J. C. Williams,‡ and W. W. Parson†

Department of Biochemistry, Box 357350, University of Washington, Seattle, Washington 98195, and Department of Chemistry and Biochemistry, Arizona State University, Tempe, Arizona 85287

Received: October 27, 1998; In Final Form: January 26, 1999

The photosynthetic bacterium *Rhodobacter sphaeroides* contains a light-harvesting antenna complex (LH2) with a ring of interacting bacteriochlorophyll molecules (B850). Excitation of membrane-bound LH2 complexes with low-intensity, femtosecond pulses causes changes in absorption and stimulated emission that initially depend on the excitation wavelength but relax to a quasiequilibrium with a time constant of 100 ± 20 fs. Excitation on the blue side of the B850 absorption band is followed by a shift of the signals to longer wavelengths and a decrease in amplitude, whereas the relaxations following excitation on the red side consist mainly of a decrease in amplitude. The signals have an apparent initial anisotropy of approximately 0.5 when the complex is excited with broadband pulses, and 0.35−0.4 with narrower pulses. The anisotropy decays to 0.1 with a time constant of about 30 fs. The anisotropies are similar at wavelengths on either side of the absorption band and are relatively insensitive to the excitation wavelength. Contributions of coherent pump−probe coupling and perturbed free induction decay to the measured anisotropies are considered. Pump−probe coupling could increase the initial anisotropy but cannot account for the decay kinetics. Using a density-matrix formalism, we show that the initial light-induced signals are consistent with coherent excitation of multiple exciton levels in an inhomogeneous ensemble of LH2 complexes and that the main features of the spectral relaxations and the anisotropy can be explained by electronic dephasing and thermal equilibration within the manifold of exciton levels.

Introduction

Photosynthetic organisms contain pigment−protein "antenna" complexes that absorb light and transfer energy efficiently and rapidly to the photochemical reaction center. The peripheral antenna complex [light-harvesting complex 2 (LH2)] from the purple, photosynthetic bacteria *Rhodopseudomonas acidophila* strain 10050 contains nine copies of each of two polypeptides (α and *β*), 27 bacteriochlorophyll *a* (BChl *a*) molecules, and 18 carotenoids in a cylindrical structure with C_9 crystallographic symmetry.[1] Eighteen of the BChls are arranged in a ring with a radius of about 25 Å. These molecules are oriented so that the bacteriochlorin ring normals are approximately perpendicular to the symmetry axis and their long-wavelength (Q_y) transition dipoles lie close to the plane of the ring. The other nine BChls form an outer ring that is displaced along the symmetry axis. The LH2 complex from the widely-studied species *Rhodobacter sphaeroides* probably contains similar rings of pigments. An LH2 complex with C_8 symmetry is found in *Rhodospirillum molischianum*.[2]

LH2 complexes typically have absorption bands in the regions of 800 and 850 nm. Semiempirical molecular orbital calculations based on the *Rps. acidophila* crystal structure indicate that the major ring of eighteen BChls accounts for the long-wavelength band while the outer ring of nine BChls is responsible for the 800 nm band.[3,4] The BChls in the inner and outer rings can, therefore, be termed the "B850" and "B800" pigments, respectively.

The absorption, circular dichroism, and hole-burning spectra of the LH2 complex are reproduced reasonably well by theoretical treatments that consider exciton states of the entire complex but invoke moderate disorder in the excitation energies of the individual BChls.[3−6] The red shift of the 850 nm absorption band relative to the Q_y transition of BChl in vitro (770 nm) appears to reflect a combination of excitonic coupling,[3,4] pigment−protein interactions,[7] distortions of the BChl macrocycles,[4,8] and, to a minor extent, mixing with charge-transfer transitions.[4] In a homogeneous system the wave function of the lowest exciton state would be distributed almost uniformly around the B850 ring, and because the Q_y transition dipoles of the B850 BChls all lie approximately in the plane of the ring, the dipole strength for excitation to this state would be very small. Most of the dipole strength of the B850 band would come from a degenerate pair of orthogonally polarized transitions at slightly higher energy.[3,4] However, energetic or structural disorder that disrupts the symmetry of the complex will cause excitations to localize on smaller subsets of the pigments, making both the low-energy transition and transitions at higher energies weakly allowed.[9−15] Evidence for such disorder has come from hole-burning spectroscopy: excitation on the red edge of the absorption band burns a narrow hole that has been assigned to the lowest exciton state.[9]

Additional evidence for disorder in the LH2 complex comes from the observation that the radiative rate constant is nearly independent of temperature.[16] In a homogeneous system the emission should drop to zero at low temperatures. The flourescence properties thus suggest that emission occurs from a relatively localized excited state, while the absorption, circular

* E-mail address for correspondence: ngrjn@u.washington.edu.
† University of Washington.
‡ Arizona State University.

10.1021/jp984236p CCC: $18.00
Published on Web 03/09/1999

dichroism, and hole spectra appear to require more delocalized exciton states. The paradox probably results in part from the different time scales probed by conventional absorption and emission spectroscopies. In hole-burning studies, excitation on the blue side of the B850 absorption band results in a broad hole that covers essentially the entire band, suggesting that the excited complex relaxes within the manifold of exciton levels on a sub-picosecond time scale.[9] Because the spontaneous fluorescence has a lifetime of several hundred picoseconds in the absence of the reaction center, measurements of fluorescence would report mainly on times following this relaxation. The nature of the rapid relaxation is of interest because it bears on how photosynthetic antenna complexes absorb and transfer energy and because it may provide an experimental window to protein dynamics on very short time scales.

To explore how the excited LH2 complex evolves with time, we previously measured the changes in absorbance and stimulated emission caused by excitation with 35 fs pulses centered at 875 nm.[17] The spectra included an absorbance increase due to excited-state absorption (ESA) and a negative feature at longer wavelengths due to stimulated emission (SE) and bleaching of ground-state absorption (GSB). Both features underwent substantial relaxations on the time scale of 10−100 fs. We also observed an anomalously large initial anisotropy (∼0.7) in the bleaching and stimulated-emission signal, which decayed to 0.1 on the same time scale as the spectral relaxations. We interpreted these results in the simple model of a homogeneous system in which excitations are delocalized over the whole ring. The high initial anisotropy was ascribed to coherent excitation of a degenerate pair of allowed states, and the relaxations to electronic dephasing and equilibration with a forbidden state at lower energies.

In the present study, we investigate the effects of exciting the LH2 complex with spectrally narrower excitation pulses on either the blue or red side of the B850 absorption maximum. We also describe more extensive measurements of anisotropy with finer time resolution, explore how the measured anisotropy depends on the excitation and detection wavelengths, and consider the effects of perturbed free induction decay and coherent coupling of the pump and probe pulses. Finally, we show that the main features of the results can be reproduced well by a theoretical treatment that considers electronic dephasing and thermal equilibration of exciton levels in an ensemble of systems with moderate disorder.

Methods

Experimental. A Ti:sapphire laser described previously[17] provided excitation and probe pulses at a repetition rate of 100 kHz. The pump pulses had a maximum energy of approximately 0.5 nJ. Their center wavelength and spectral width were controlled by a moveable slit. The probe pulses, which had an energy of about 50 pJ, had a full width at half-maximal amplitude (fwhm) of approximately 25 fs at the sample, assuming a $\mathrm{sech}^2(t)$ shape. The fwhm of the cross correlation of the pump and probe pulses was approximately 60 fs. After passing through the sample, the probe beam was dispersed by a spectrometer with a bandwidth of 5 nm and recorded by a photodiode and lock-in amplifier.[17]

Although extracavity prisms were used for dispersion compensation, the pulses still retained some negative chirping. When the center of the pump pulse was tuned from 830 to 870 nm (20 nm on either side of the B850 band), the peak of the pump−probe cross-correlation function shifted by 18 fs. The shift was approximately linear with wavelength. Chirping of the probe pulse causes the actual pump−probe delay to increase with increasing wavelength. Correcting for this effect increases the signals slightly at early times on the blue side of the spectrum, and decreases the signals at early times on the red side, but the correction is relatively small. The data presented below are uncorrected.

For anisotropy measurements, signals with parallel and perpendicular polarization of the pump and probe beams were recorded at each setting of the delay stage by rotating the polarization of the pump beam with a half-wave plate. This method is preferable to collecting the time-dependent parallel and perpendicular signals separately, because errors in the stage position are identical for both signals and thus affect the measured anisotropy only minimally. The anisotropies that we reported previously[17] probably were overestimated as a result of an error of $\sim 1\ \mu$m in reproducing the stage position. Such an error also would affect the apparent decay kinetics of the anisotropy.

Because measurements of the transient difference spectra require dispersing the probe beam after the sample, the preferred method of examining the anisotropy is to vary the pump polarization as we have done. However, the polarization is rotated by retarding the optical component parallel to the slow axis of the retarder plate, which introduces a slight delay and temporal broadening of the pump pulse for one polarization relative to the other. Although this problem appears not to have been described previously, we observed the effect clearly in the pump−probe cross-correlation traces. The observed retardation corresponded to ∼0.7 fs or $\sim\lambda/4$, as expected. We neglected this effect in the analysis of the anisotropy data because attempting to correct for it probably would introduce other errors of a similar magnitude. The retardation was such (excitation occurred slightly earlier with perpendicular polarization than with parallel) that the calculated initial anisotropies are *lower* limits. Partial depolarization of the pump and/or probe beam by the mirrors between the half-wave plate and the sample also can cause an underestimate of the true anisotropy (see below).

We checked the anisotropy signals for a dependence of the amplitudes or decay kinetics on the excitation intensity, and found none. For this, the pulse energies were reduced by adjusting the radio-frequency power applied to the Bragg crystal in the pulse selector.[17] This method preserves the shapes and spectra of the pulses, but decreases the signal/noise ratio because it reduces both the pump and probe intensities.

Chromatophores from *Rb. sphaeroides* strain ΔQBALM/Q, which contains LH2 but not reaction centers or LH1 complexes, were prepared as described[17] and were diluted in 50 mM TRIS-HCl, pH 8.0, to an absorbance of 0.2 ± 0.1 at 850 nm. Cuvettes with a pathlength of 0.1 mm were used for measurements of spectral relaxations and 0.2 mm for anisotropy measurements. The signals were larger with the 0.2 mm cuvettes because the pump and probe beams overlapped across a distance of about 0.15 mm, but otherwise were not noticeably different. All measurements were made at room temperature. Data were analyzed globally by singular value decomposition using methods described previously.[17]

Theoretical. Exciton states of the LH2 complex were evaluated on the basis of the *Rp. acidophila* crystal structure as described by Alden et al.[4] but with the interaction matrices restricted to the Q_y transitions of the 18 B850 BChls; charge-transfer transitions and the Q_x, B_y, and B_x transitions were omitted, along with all transitions of the B800 pigments. This simplification reduces the interaction matrix for the singly-excited complex (**U**) from 252×252 to 18×18 with relatively

minor effects on the calculated absorption spectrum in the 850 nm region. The mean values of the monomer excitation energies were set at 12450 cm^{-1} for BChls bound to α polypeptides and 12350 cm^{-1} for those bound to β polypeptides. (We have not investigated the importance of retaining the small calculated[4] difference between the transition energies of the BChls bound to the α and β polypeptides in the present study, but it probably is minor.) Off-diagonal elements were calculated with the dielectric screening parameters $n^2 = 2$ and $r_o = 4$ Å^4 and were increased uniformly by 18%. This scaling put the interaction between an $\alpha\beta$ pair of BChls (the largest off-diagonal terms of **U**) at 300 cm^{-1}.

The 171 × 171 interaction matrix for a doubly excited system (**V**) was constructed from **U** as described by van Amerongen and Struve[18] and Pullerits et al.[19] **V** includes states in which an individual BChl molecule is doubly excited, in addition to states in which Q_y excitations reside simultaneously on two different BChls. Excitation of an individual BChl from the first to the second excited state was assigned a transition energy 100 cm^{-1} greater than the Q_y excitation and a transition dipole parallel to the Q_y transition dipole.[18,20] The ratio of the magnitudes of the transition dipoles for the first and second excitations was taken to be 0.5. (The results do not depend strongly on this ratio because most of the excited-state absorption involves the more numerous states in which two different BChls are excited.) Eigenstates of singly and doubly excited complexes were obtained by diagonalizing **U** and **V** separately.

The ground-state absorption spectrum was calculated as described,[4] but with the simplifications that (1) all transitions, including the lowest, were assigned a Lorentzian homogeneous line shape with a fwhm of 250 cm^{-1}, (2) no vibronic structure was included, and (3) mixing of doubly excited states with the ground state was neglected. Inhomogeneous broadening was introduced by giving the monomer transition energies (the diagonal terms of **U**) Gaussian disorder with a standard deviation (σ) of 200 or 300 cm^{-1} (fwhm = $\sqrt{8\ln 2}\ \sigma$ = 471 or 706 cm^{-1}). This gave the diagonal terms of **V** correlated disorder with a standard deviation $\sqrt{2}\ \sigma$.

To calculate the light-induced changes in absorption and emission, a reduced density matrix $\boldsymbol{\rho}$ was defined for a singly-excited system in the exciton representation, and then averaged over orientations and a distribution of monomer transition energies for an ensemble of such systems. The ground-state system was assumed to be excited by a pulse with a spectral width similar to those of the pulses used experimentally (see Figure 1) and peaking either 184 cm^{-1} to the blue or 222 cm^{-1} to the red of the calculated absorption maximum. To represent a coherent superposition of the allowed "one-exciton" states, the density matrix at time $t = 0$ was taken to be

$$\rho_{a,b}(t=0,\hat{e}_i) = \Gamma^{-1}(\hat{e}_i\cdot\hat{\mu}_a)(\hat{e}_i\cdot\hat{\mu}_b)J_{ab} \tag{1a}$$

Here $\hat{e}_i$, $\hat{\mu}_a$, and $\hat{\mu}_b$ are unit vectors parallel to the electric field of the pump pulse and to the transition dipoles ($\vec{\mu}_a$ and $\vec{\mu}_b$) for excitation from the ground state to exciton states *a* and *b*; J_{ab} is a spectral overlap integral of the pump pulse with the two excitation spectra; and Γ is a normalization factor. The spectral overlap integrals are

$$J_{ab} = |\vec{\mu}_a||\vec{\mu}_b| \int I(\nu)\{W_a(\nu)W_b(\nu)\}^{1/2}\mathrm{d}\nu \tag{1b}$$

where $I(\nu)\mathrm{d}\nu$ is the excitation intensity at frequency ν and $W_a(\nu)$ is the normalized Lorentzian line shape for excitation to state *a*. The use of the geometric mean $(W_aW_b)^{1/2}$ for the off-diagonal terms of $\boldsymbol{\rho}$ at time 0 follows Rahman et al.[21]

The normalization factor Γ is

$$\Gamma = \langle\sum_a(\hat{e}_i\cdot\hat{\mu}_a)^2J_{aa}\rangle_{O,E} = \frac{1}{3}\langle\sum_a J_{aa}\rangle_E \tag{1c}$$

where $\langle...\rangle_O$ indicates averaging over all orientations with respect to $\hat{e}_i$ and $\langle...\rangle_E$ denotes averaging over the distribution of the monomer transition energies. With this normalization, $\mathrm{Tr}\{\langle\boldsymbol{\rho}\rangle_{O,E}\} = 1$ for an inhomogeneous ensemble of randomly oriented systems.

The intensity of SE from an orientationally averaged exciton state *a* at time zero is

$$F_a(\nu,\hat{e}_i,\hat{e}_f) = C\{\sum_{b=1}^{18}\langle(\hat{e}_f\cdot\vec{\mu}_a)(\hat{e}_f\cdot\vec{\mu}_b)\rho_{a,b}(0,\hat{e}_i)\rangle_O\}W_a(\nu) = C\Gamma^{-1}\{\sum_{b=1}^{18}\langle(\hat{e}_i\cdot\hat{\mu}_a)(\hat{e}_i\cdot\hat{\mu}_b)(\hat{e}_f\cdot\hat{\mu}_a)(\hat{e}_f\cdot\hat{\mu}_b)\rangle_O \times (J_{ab})^{1/2}|\vec{\mu}_a||\vec{\mu}_b|\}W_a(\nu) \tag{2a}$$

where $\hat{e}_f$ is the probe polarization and *C* is a constant that depends on the pump and probe intensities, the refractive index of the medium, local field corrections, and physical constants. The sum runs over all the one-exciton states. We used the same homogeneous lineshape $W_a(\nu)$ for SE or ESA as for ground-state absorption (fwhm = 250 cm^{-1}).

Excited-state absorption from state *a* to a doubly excited ("two-exciton") state η at time zero is given similarly by

$$A_{a\eta}(\nu,\hat{e}_i,\hat{e}_f) = C\Gamma^{-1}\{\sum_{b=1}^{18}\langle(\hat{e}_i\cdot\hat{\mu}_a)(\hat{e}_i\cdot\hat{\mu}_b)(\hat{e}_f\cdot\hat{\mu}_{a\eta})(\hat{e}_f\cdot\hat{\mu}_{b\eta})\rangle_O \times (J_{ab})^{1/2}|\vec{\mu}_{a\eta}||\vec{\mu}_{b\eta}|\}W_{a\eta}(\nu) \tag{2b}$$

where $\vec{\mu}_{a\eta}$ and $W_{a\eta}(\nu)$ are the transition dipole and line shape for the excitation $a \rightarrow \eta$.

Setting the off-diagonal terms of $\boldsymbol{\rho}$ to zero gives an incoherent mixture of one-exciton states with the same initial populations. The sums in eqs 2a and b then reduce to

$$F_a(\nu,\hat{e}_i,\hat{e}_f) = C\Gamma^{-1}\langle(\hat{e}_i\cdot\hat{\mu}_a)^2(\hat{e}_f\cdot\hat{\mu}_a)^2\rangle_O J_{aa}|\vec{\mu}_a|^2W_a(\nu) \tag{3a}$$

and

$$A_{a\eta}(\nu,\hat{e}_i,\hat{e}_f) = C\Gamma^{-1}\langle(\hat{e}_i\cdot\hat{\mu}_a)^2(\hat{e}_f\cdot\hat{\mu}_{a\eta})^2\rangle_O J_{aa}|\vec{\mu}_{a\eta}|^2W_{a\eta}(\nu) \tag{3b}$$

Finally, if the diagonal terms of $\boldsymbol{\rho}$ are replaced by the populations for a Boltzmann equilibrium at temperature *T* (with the off-diagonal terms zero), the SE and ESA from state *a* become

$$F_a(\nu,\hat{e}_i,\hat{e}_f) = C\Gamma^{-1}\{\sum_{b=1}^{18}\langle(\hat{e}_i\cdot\hat{\mu}_b)^2(\hat{e}_f\cdot\hat{\mu}_a)^2\rangle_O J_{bb}\} \exp(-E_a/k_BT)Z^{-1}|\vec{\mu}_a|^2W_a(\nu) \tag{4a}$$

$$A_{a\eta}(\nu,\hat{e}_i,\hat{e}_f) = C\Gamma^{-1}\{\sum_{b=1}^{18}\langle(\hat{e}_i\cdot\hat{\mu}_b)^2(\hat{e}_f\cdot\hat{\mu}_{a\eta})^2\rangle_O J_{bb}\} \exp(-E_a/k_BT)Z^{-1}|\vec{\mu}_{a\eta}|^2W_{a\eta}(\nu) \tag{4b}$$

where E_a is the energy of exciton state *a*, k_B is the Boltzmann constant, and $Z = \sum_{a=1}^{18}\exp(-E_a/k_BT)$. The terms of the sums

in eqs 4 represent preparation of state *b* by the excitation pulse, followed by internal conversion to state *a*. Note that the Boltzmann equilibrium described by these equations pertains to an individual LH2 complex with a particular set of transition energies. Thermal equilibration of the entire ensemble would remove all memory of the excitation wavelength and polarization.

The contribution of exciton state *a* to GSB includes a sum similar to those in eqs 4:

$$G_a(\nu,\hat{e}_i,\hat{e}_f) = C\Gamma^{-1}\{\sum_{b=1}^{18}\langle(\hat{e}_i\cdot\hat{\mu}_b)^2(\hat{e}_f\cdot\hat{\mu}_a)^2\rangle_O J_{bb}\}|\vec{\mu}_a|^2 W_a(\nu) \quad (5)$$

This is independent of the dephasing and thermalization of $\boldsymbol{\rho}$.

After averaging over the distribution of monomer energies, the total signal for an inhomogeneous ensemble is

$$S(\nu,\hat{e}_i,\hat{e}_f) = \langle\sum_a\{-G_a(\nu,\hat{e}_i,\hat{e}_f) - F_a(\nu,\hat{e}_i,\hat{e}_f) + \sum_\eta A_{a\eta}(\nu,\hat{e}_i,\hat{e}_f)\}\rangle_E \quad (6)$$

The orientational averages in F_a, $A_{a\eta}$, and G_a depend on the polarization of the probe beam relative to the pump. Expressions for these averages are given in the Appendix. F_a and $A_{a\eta}$ also depend on whether the excitation is coherent (eqs 2a and 2b), incoherent (3a and b), or thermalized (4a and b). This distinction is idealized because, in an actual measurement, dephasing and thermalization of $\boldsymbol{\rho}$ are coupled processes and are convoluted with the excitation pulse.

Finally, the isotropic signal $K(\nu)$ and anisotropy $r(\nu)$ are

$$K(\nu) = S(\nu,\hat{x},\hat{x}) + 2S(\nu,\hat{x},\hat{y}) \quad (7a)$$

and

$$r(\nu) = \frac{S(\nu,\hat{x},\hat{x}) - S(\nu,\hat{x},\hat{y})}{S(\nu,\hat{x},\hat{x}) + 2S(\nu,\hat{x},\hat{y})} \quad (7b)$$

where $\hat{x}$ and $\hat{y}$ indicate polarization along orthogonal laboratory axes. Calculations of $K(\nu)$ and $r(\nu)$) were repeated for 1000 iterations of the Monte Carlo procedure used to provide diagonal disorder in **U** and **V**, and the calculated spectra were averaged in bins with a resolution of 10 cm^{-1}.

To express the enhancement of the isotropic emission strength of the LH2 complex compared to the emission strength of monomeric BChl *a*, it is useful to define the dimensionless ratio

$$L_e(t) = \langle F_{\|} + 2F_{\perp}\rangle_{O,E}/|\vec{\mu}^m|^2 \quad (8a)$$

where $|\vec{\mu}^m|^2$ is the Q_y dipole strength for BChl *a* in solution (we used 50 D^2),[4] $F_{\|} = F(t,\hat{x},\hat{x})$, $F_{\perp} = F(t,\hat{x},\hat{y})$, and

$$F(t,\hat{e}_i,\hat{e}_f) = \sum_a\sum_b(\hat{e}_f\cdot\vec{\mu}_a)(\hat{e}_f\cdot\vec{\mu}_b)\rho_{a,b}(t,\hat{e}_i) \quad (8b)$$

The sums in eq 8b again run over the exciton states. Evaluating the orientational averages gives

$$L_e^{coh} = \langle\sum_a\sum_b(\hat{\mu}_a\cdot\hat{\mu}_b)^2|\vec{\mu}_a||\vec{\mu}_b|(J_{ab})^{1/2}\rangle_E/(3\Gamma|\vec{\mu}^m|^2) \quad (9a)$$

for the coherently excited ensemble at time zero and

$$L_e^{inc} = \langle\sum_a|\vec{\mu}_a|^2 J_{aa}\rangle_E/(3\Gamma|\vec{\mu}^m|^2) \quad (9b)$$

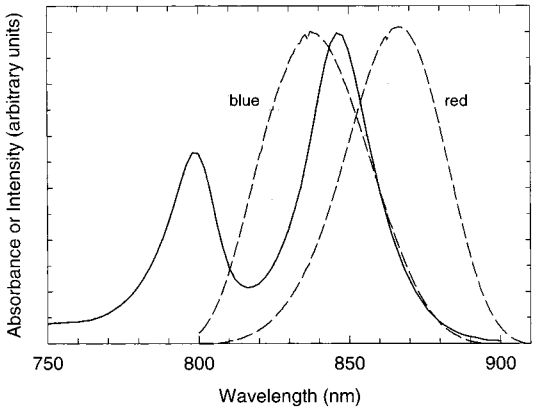

Figure 1. Absorption spectrum of chromatophores from strain ΔQBALM/Q (solid line) and intensity spectra of the "blue" and "red" pump pulses (dashed lines).

and

$$L_e^{therm} = \langle(\sum_a|\vec{\mu}_a|^2 e^{-E_a/k_BT}Z^{-1})(\sum_b J_{bb})\rangle_E/(3\Gamma|\vec{\mu}^m|^2) \quad (9c)$$

for the incoherent and thermalized excitations, respectively. As above, the thermalization in eq 9c is restricted to individual LH2 complexes.

L_e^{coh}, L_e^{inc}, and L_e^{therm} depend on the geometry, electronic structure and inhomogeneity of the complex and, in the case of L_e^{therm}, on the temperature. With broadband excitation pulses, L_e^{inc} and L_e^{therm} both go to 1 if the electronic coupling between the BChls is set to zero so that the exciton transition dipoles are transition dipoles of individual molecules ($|\vec{\mu}_a|^2 = |\vec{\mu}_b|^2 = |\vec{\mu}^m|^2$). L_e^{coh} generally is greater than 1 even for systems with no electronic coupling, as long as the monomer transition dipoles have fixed orientations with respect to each other. For 18 noninteracting BChls in a planar arrangement with C_9 or C_{18} symmetry, L_e^{coh} would be $(18)(1/2) = 9$.

Results

1. Spectral Relaxations. Figure 1 shows the absorption spectrum of chromatophores containing the LH2 complex. Also shown are the spectra of pump pulses centered at 838 and 868 nm, which we will call "blue" and "red" excitation pulses, respectively. The excitation probability (product of the pump and absorption spectra) peaks at 843 nm with the blue pulses and 855 nm with the red. In a system with moderate disorder, both pump pulses would excite predominantly the two or three most strongly allowed transitions in the region of 850 nm. The red pulses also would excite the weakly allowed, low-energy transition, whereas the blue pulses could also excite some of the higher energy transitions.

The upper parts of Figure 2 show the changes in isotropic absorbance and stimulated emission measured at several times after a red or blue excitation pulse. In these measurements, the probe pulses were polarized at the magic angle (54.7°) relative to the pump. Both types of excitation result in ground-state bleaching (GSB) and stimulated emission (SE) in the region of 850 nm and a broad band of excited-state absorption (ESA) near 830 nm. The arrows indicate how the signals change with time. After blue excitation (Figure 2A) the negative feature shifts to longer wavelengths, while SE grows in around 880 nm and the ESA declines. Following red excitation (Figure 2B) the positive and negative signals decrease simultaneously, with little shifting of the spectrum.

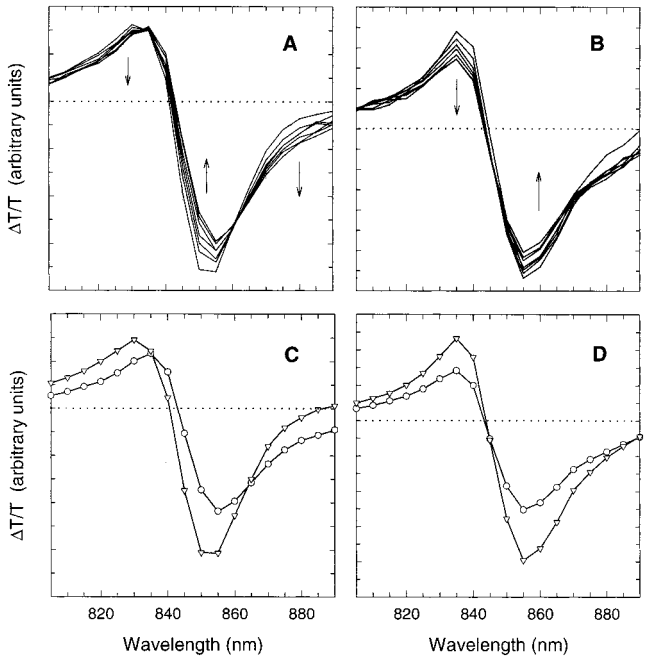

Figure 2. Upper Parts: Absorbance difference spectra measured at delay times 25, 50, 75, 100, 150, 200, and 350 fs following excitation with pulses on the blue (A) or red (B) side of the B850 absorption band. The dotted horizontal lines mark zeros of the ordinate scale. Arrows point in the direction of increasing time delay. The maximum fractional absorbance change was $<10^{-3}$ in all cases. Lower Parts: Difference spectra at $t = 0$ (▽) and ∞ (○) following the blue (C) and red (D) excitations, reconstructed from the experimental data by singular-value decomposition and global kinetic analysis. The calculated relaxation times were 110 and 80 fs for the blue and red excitations, respectively.

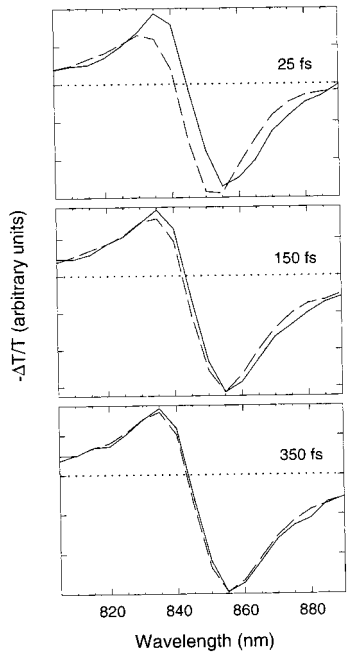

Figure 3. Difference spectra measured at 25, 150, and 350 fs following red (solid lines) and blue (dashed lines) excitations. Zero time was taken to be the maximum of the pump-probe intensity cross-correlation trace. The spectra were scaled to normalize their amplitudes at 350 fs.

Figure 3 compares difference spectra measured at 25, 150, and 350 fs after the two excitation pulses. At 25 fs, the GSB/SE signals generated by blue excitation peak about 5 nm to shorter wavelengths than the signals seen with red excitation. The ESA is weaker relative to the bleaching with the blue excitation and also is blue shifted by about 5 nm. These differences have largely disappeared by 150 fs, and except for a small difference that decays more slowly (see below), the two spectra are virtually identical at 350 fs. Temporal signals integrated over all detection wavelengths were virtually superimposable for red and blue excitation (not shown).

We typically collected 100 spectra for each excitation, with delay times extending from −150 to +350 fs and wavelengths ranging from 805 to 890 nm. Singular value decomposition was used to separate the data matrix into a sum of products of the form

$$S(\lambda,t) = \sum_i \xi_i(\lambda)\chi_i(t)\gamma_i \qquad (10)$$

where $\xi_i(\lambda)$ and $\chi_i(t)$ are functions of wavelength and time, respectively, and γ_i is the singular value amplitude of component i.[17] Only the first few components were retained (two for red excitation and three for blue). The time courses of the next one or two components had first- or second-derivative shapes and decayed to zero within the period of pump−probe overlap. These were rejected because analyses of simulated data indicated that they probably represent coherent interaction between the pump and probe electric fields in the sample and frequency chirp in the probe pulse. (In our previous study,[17] we retained an additional short-lived component. This decreased the dominant time constant returned in the next stage of the analysis.) All the remaining components had very small singular values and waveforms that appeared to reflect only random noise. The significant kinetic waveforms ($\chi_i(t)$) were fit globally to a multiexponential function convoluted with the pump−probe cross-correlation function. An accurate fit usually required three or four exponential terms plus a constant. However, the first few terms probably represented residual effects of pump−probe coherence and/or chirping because they had time constants of less than 20 fs, i.e., less than the pump−probe cross-correlation width. We therefore will discuss only the terms with lifetimes greater than 50 fs.

For data sets that extended to 350 fs, this analysis led to a satisfactory description of the results of either red or blue excitation in terms of a single relaxation. The fits returned a somewhat shorter relaxation time constant for red excitation (83 fs) than for blue (114 fs). Fitting the signals at individual wavelengths separately rather than globally gave shorter time constants, probably because of the greater difficulty of removing contributions from chirping and pump−probe coherence. Adding another decay component did not improve the global fits significantly. However, a similar global analysis of data with time steps of 50 fs and delays extending to 5 ps returned a small additional component with a relaxation time of 1.2 ± 0.4 ps.

Difference spectra for any given delay time can be reconstructed from the significant terms of the sum in eq 10.[17] The spectra for times following the period of pump-probe overlap agreed closely with experimental spectra. Spectra for delay times $t = 0$ and ∞ are shown in the lower panels of Figure 2. With either red or blue excitation, the relaxation reduces the amplitudes of both the positive and negative features by approximately 30% and broadens the negative feature on the long-wavelength side. After blue excitation, the positive and negative features both shift to longer wavelengths by about 3 nm.

2. Anisotropy. The anisotropy of the signals was measured under several different conditions. In one set of experiments we excited samples at 827, 850, or 872 nm and measured the anisotropy at 860 nm. In another, we excited samples with the entire laser bandwidth (here a fwhm of 70 nm) to maximize

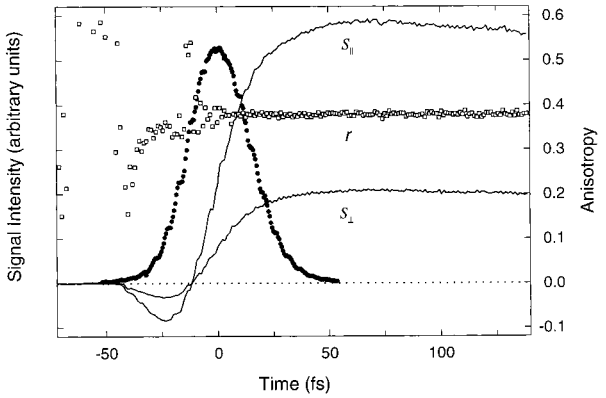

Figure 4. Changes in absorbance and stimulated emission measured with IR-132 in dimethyl sulfoxide with probe beams polarized parallel ($S_{||}$) or perpendicular ($S_{\perp}$) to the pump polarization. Excitation was with broadband pulses centered at 842 nm (fwhm ≈ 90 nm) and detection was at 875 ± 2.5 nm. Also shown are the pump−probe cross-correlation function (●) and the raw anisotropy (r, □) calculated directly from the signals. The apparent decrease in r at $t < 0$ may reflect the different retardation of the pump beam in the two polarizations (see Methods).

the time resolution and measured the anisotropy at various wavelengths between 820 and 875 nm; we also measured the anisotropy with an undispersed probe beam peaking at 832 or 845 nm. In all cases, the "raw" anisotropy of the signals, $(S_{||} - S_{\perp})/(S_{||} + 2S_{\perp})$ where $S_{||}$ and $S_{\perp}$ are signals measured with pump and probe polarizations parallel and perpendicular, decayed from an initial value between 0.35 and 0.55 to a value close to 0.1 on a time scale of approximately 30 fs. We checked for saturation effects in the signal by reducing the intensity of the pump and probe beams by a factor of ∼3 and obtained an anisotropy decay that was not significantly different. We also eliminated pump−pulse-induced Kerr lensing[22] as an artifactual source of the rapid decay of anisotropy by comparing results obtained at 850 nm with the detection wavelength selected by either a monochromator or an interference filter. In principle, the narrow entrance slit of the monochromator might pass different amounts of the probe light depending on the shape of the pump-induced lens, which would vary with the pump polarization. However, the results again were identical to within the noise level of the measurements.

As a test of the procedure for measuring anisotropy, we examined the signals generated by exciting the laser dye IR-132 in dimethyl sulfoxide. Figure 4 shows the results. The raw anisotropy was essentially constant at 0.38 even through most of the period of pump−probe overlap. The difference between 0.38 and the theoretical value of 0.40 may be due to a slight depolarization of the pump and probe beams by the mirrors between the half-wave plate and the sample. The decrease in the apparent anisotropy at $t < -20$ fs could reflect the delay of ∼0.7 fs associated with rotating the pump polarization.

A determination of the true anisotropy of the LH2 signals at early times is problematic because of coherent pump−probe coupling (PPC) and perturbed free-induction decay (PFID). The PFID signal in the probe direction arises because the probe pulse generates ground-excited electronic coherence that radiates at the nominal transition frequency.[23] If the pump pulse follows the probe during the period of electronic dephasing, it interrupts the free induction decay. This effect is seen as a decay of the coherence signal in the direction of $t < 0$. The coherence signal is heterodyned with the probe pulse, giving rise to oscillations as a function of the frequency detuning.[23] Assuming that the transition dipoles of the sample do not rotate during the period of electronic dephasing, the PFID and PPC signals will have anisotropies of 0.4. They therefore can interfere with measurements of anisotropies that differ from this value.

To remove the effects of PFID, the data were analyzed by first constructing isotropic and polarization−difference signals as $S_{||} + 2S_{\perp}$ and $S_{||} - S_{\perp}$, respectively. The isotropic signal was fit by non-linear least-squares to the function[24]

$$K(t) = [K_1(t) + K_2(t)] \otimes P(t + \delta) \tag{11a}$$

where

$$K_1(t) = (1 - \theta(t))\, a_o \exp\{t/T_2\}\cos(\omega t) \tag{11b}$$

and

$$K_2(t) = \theta(t) \sum_{i=1}^{N} a_i \exp\{-t/\zeta_i\} \tag{11c}$$

In eq. 11a, ⊗ denotes a convolution integral, $P(t)$ is the measured pump−probe crosscorrelation function, and δ is an adjustable time shift. In eqs 11b and c, $\theta(t)$ is the Heaviside step function (0 for $t < 0$ and 1 for $t \geq 0$), ω is the frequency detuning of the peak of the probe spectrum from the 850 nm absorption peak, the a_i are amplitudes, ζ_i's are time constants, and T_2 is a time constant for decay of electronic coherence. We assume here that the electronic dephasing can be described adequately by a single exponential decay. $K_2(t)$ is the multiexponential function commonly used to fit signals for $t > 0$, while $K_1(t)$ represents PFID. Terms with lifetimes less than the pump-probe cross correlation width are retained in eq 11c because here the exact form of $K_2(t)$ need not have any particular physical significance.

With $K_1(t)$ and $K_2(t)$ determined by fitting the isotropic signal, the polarization−difference signal ($S_{||} - S_{\perp}$) was fit to the function

$$D(t) = [0.4K_1(t) + r(t)K_2(t)] \otimes P(t + \delta) \tag{12}$$

Here the anisotropy of the PFID term is fixed at 0.4 and $r(t)$, the anisotropy decay that we seek, is assumed to be another multiexponential function $[r(t) = r_\infty + \sum_i r_i \exp(-t/\tau_i)]$. We assume here that the same $r(t)$ applies to all components of $K_2(t)$, which could be incorrect if $K_2(t)$ contains significant contributions from pump−probe coherence signals (see below).

Examples of the fits are shown in Figure 5 for signals measured at 830 nm (part A) and for signals measured without a monochromator in the probe beam (part B). In these experiments, the sample was excited with the full spectral width of laser pulses centered around 840 nm; the pump−probe cross-correlation traces had a typical fwhm of 32 fs. In accord with the results presented in the previous section, the fits of the isotropic signal to $K(t)$ returned a relaxation with a time constant in the range of 80−100 fs along with faster components of doubtful physical significance. The fits to both $K(t)$ and $D(t)$ were excellent at 830, 850, and 860 nm and also with the undispersed probe (see Figure 5). They were less satisfactory at 820 or 875 nm, where the signals were smaller. The time constants for the anisotropy decay measured at various wavelengths are given in Table 1. Excluding 875 nm, where the fits are poor, the data give a nearly constant value in the vicinity of 0.52 for the initial anisotropy $r(0)$. The anisotropy decays to approximately 0.1 with an apparent time constant of about 30 fs. The data at most wavelengths could be fit well by using a single exponential expression for $r(t)$, but a biexponential expression improved the fit significantly at 830 nm.

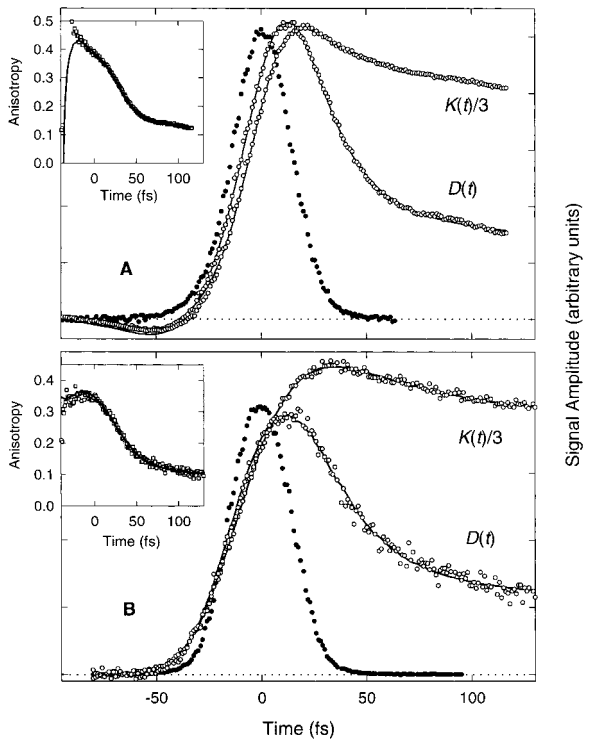

Figure 5. Isotropic [$K(t)/3$] and polarization−difference [$D(t)$] decay signals following excitation by broad-band pulses centered at 843 nm and detection at 830 nm (top part) or over the entire bandwidth of the probe pulses (bottom part). The open circles (○) are data points; the curves show the fits obtained as described in the text with the anisotropy decay parameters given in Table 1. The pump−probe cross-correlation functions are shown with filled circles (●); these are normalized arbitrarily at their peaks to be similar to the peaks of D. Time zero is the peak of the cross-correlation function. The inserts show the "raw" anisotropies obtained directly from the signals (□) and calculated from the fits to $K(t)$ and $D(t)$ (solid lines).

Contributions of PFID to the signals can be seen at negative times in Figure 5A. Here the probe wavelength was on the blue side of the B850 band and the PFID and ESA signals had opposite signs. The apparent dephasing time T_2 obtained from the data for 830, 850 and 860 nm (Table 1) had a mean value of 19 fs with a large uncertainty. PFID is less obvious in the lower panel of Figure 5, where it has the same sign as the dominant signals from GSB and SE and probably is attenuated by the integration over a broader band of wavelengths.

For comparison with the spectral-relaxation data, we also measured anisotropy decays at 860 nm following excitation with pulses centered at 872, 827, or 850 nm. The crosscorrelation fwhm of the pump and probe was approximately 40 fs, and the scan length was 400 fs. As expected, the isotropic signals were different for the three different pump wavelengths. However, the raw anisotropies obtained directly from the experimental signals were essentially indistinguishable. The anisotropy decay functions derived from the fits to $D(t)$ are collected in Table 2. Rows 2−4 in the table are the results of using a single-exponential expression for $r(t)$; rows 5−7 are two-exponential fits. The initial anisotropy had mean values of 0.37 and 0.40 in the one- and two-exponential fits, respectively, and appeared not to vary significantly with the excitation wavelength. In the one-exponential fits, the anisotropy decayed to slightly below 0.1 with a time constant of about 50 fs; with two exponentials, the time constant of the major component was 31 ± 11 fs.

The analysis described above does not consider contributions to $K_2(t)$ from coherent pump-probe coupling (PPC). In a two-level system, PPC signals have an intrinsic anisotropy of 0.4 and would not affect the measurement if the signal from GSB, ESA, and SE had a similar anisotropy. The IR-132 measurements (Figure 4) illustrate this point; here all the components of the signal have a constant anisotropy of approximately 0.4. On the other hand, if the signal from GSB, ESA, and SE had a constant but lower anisotropy, coherence signals could raise the measured anisotropy close to 0.4 during the period of pump−probe overlap. The anisotropy would decay rapidly to the lower value after this period. Contributions from PPC also could affect the apparent initial value and dynamics of an anisotropy that decays rapidly with time.

We attempted to incorporate PPC in the analysis by including a term with a time constant of zero and a fixed anisotropy of 0.4 in eqs 11 and 12. However, the fits to the experimental data were poorly determined. The convergence of the parameter values depended strongly on the initial estimates.

To evaluate the expected effects from PPC in a simple two-level system, we simulated the pump−probe spectra by calculating the induced polarization of an optically thin sample to third order in the electric field.[25−27] The dynamics of the system were modeled by a sum of two overdamped Brownian oscillators with the memory function

$$M(t) = \Delta_1^2 \exp(-t/\tau_1) + \Delta_2^2 \exp(-t/\tau_2) \qquad (13)$$

The energy correlation times, τ_1 and τ_2, were taken to be 90 fs and 15 ps, respectively, with the former representing the spectral relaxation time measured for the LH2 complex and the latter representing static inhomogeneity on the experimental time scale. Using shorter correlation times would decrease the effects of coherent pump−probe coupling. At high temperatures, the coupling strengths (Δ_i) are related to the solvent reorganization energies (λ_i) by $\Delta_i^2 = 2\lambda_i k_B T$.[(27)] Coupling strengths of $\Delta_1 = 115\ \mathrm{cm}^{-1}$ and $\Delta_2 = 140\ \mathrm{cm}^{-1}$ were chosen to give bandwidths of about 410 cm^{-1} for the calculated absorption and emission spectra and a peak separation of about 130 cm^{-1} in accord with the experimentally measured Stokes shift for the LH2 complex.[28] Isotropic spectra for PFID, PPC, SE, and GSB were calculated separately for various pump−probe delay times,[26,27] using Gaussian pump and probe pulses with widths comparable to those of the pulses used experimentally. Temporal profiles were constructed by integrating the calculated spectra over the experimental detection window of 5 nm around a given detection wavelength.

The sum of the calculated isotropic SE plus GSB was fitted to the convolution of the pump−probe cross correlation with an isotropic response function, $S(t)$, consisting of a single exponential term plus a constant. To generate the components with parallel or perpendicular polarization, the $S(t)$ returned by this fit was multiplied by $(1 + 2r(t))$ or $(1 - r(t))$, where $r(t)$ is an assumed anisotropy decay function, and the product was reconvoluted with the pump−probe cross-correlation function. The components of the PFID and PPC signals with parallel and perpendicular polarization were obtained directly from the corresponding isotropic signals (without the deconvolution−reconvolution procedure) by assuming a constant anisotropy of 0.4. Finally, all the contributions were combined to give total signals ($S_\parallel$ and $S_\perp$) that were used to calculate the raw anisotropy.

Figure 6 shows the results of this calculation for the assumed anisotropy decay function $r(t) = 0.29 \exp(-t/\tau) + 0.11$ with $\tau = 33$ fs. The raw anisotropy obtained experimentally for the LH2 complex under similar conditions is shown for comparison. If the contribution from PPC was omitted, the calculated anisotropy decreased slightly at times near the peak of the excitation pulse (see Figure 6); however, an anisotropy curve

TABLE 1: Best-Fit Parameters to Anisotropy Measured at Various Wavelengths after Broad-Band Excitation

detection wavelength (nm)	T_2 (fs)	r_1	τ_1 (fs)	r_2	τ_2 (fs)	r_∞	$r(0)$[d]
820[a,b]	8	0.49	42			0.07	0.56
830[a]	35	0.38	19	0.14	515	0.01	0.53
850[a]	16	0.43	29			0.10	0.53
860[a]	6	0.42	34			0.10	0.52
875[a,b]	12	0.60	43			0.09	0.69
broad-band[c]	14 ± 6	0.37 ± 0.02	26 ± 1			0.11 ± 0.01	0.48 ± 0.02

[a] Detection bandpass was 5 nm. [b] Fits to the polarization−difference signal were poor at these wavelengths. [c] The probe pulse was not dispersed after the sample; the values are averages of measurements on two samples. [d] Initial anisotropy: $r(0) = r_1 + r_2 + r_\infty$.

TABLE 2: Best-Fit Parameters to Anisotropy Measured at 860 nm after Excitation at Various Wavelengths

excitation wavelength[a]	r_1	τ_1 (fs)	r_2	τ_2 (fs)	r_∞	$r(0)$[b]
827[c]	0.26	45			0.08	0.34
850[c]	0.26	51			0.09	0.35
872[c]	0.32	48			0.09	0.41
827[d]	0.20	19	0.13	83	0.08	0.41
850[d]	0.25	42	0.10	846[e]	0.01[e]	0.36
872[d]	0.21	31	0.13	82.3	0.09	0.43

[a] Peak (nm). [b] Initial anisotropy: $r(0) = r_1 (+ r_2) + r_\infty$. [c] Anisotropy fit to a single-exponential function. [d] Anisotropy fit to a biexponential function. [e] Not determined reliably (the data extend to 350 fs).

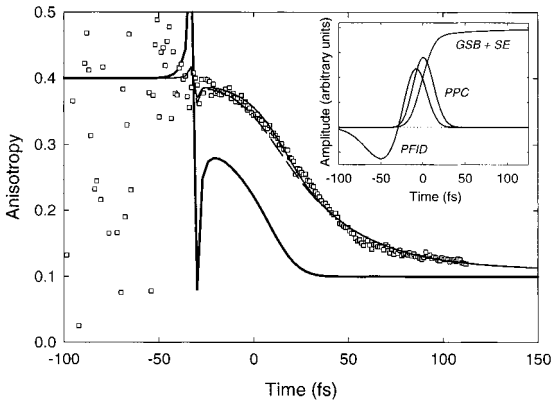

Figure 6. Raw anisotropy of the signals calculated from the third-order polarization of a two-state system with $\Delta_1 = 115$ cm^{-1}, $\Delta_2 = 140$ cm^{-1}, $\tau_1 = 90$ fs, and $\tau_2 = 15$ ps. The system is excited with a broadband pulse centered at the absorption maximum, and is probed about 10 nm to the red. The curves shown with solid lines include PPC, PFID, GSB and SE; PPC is omitted in the calculations shown with a dashed line. The GSB+SE signal was assumed to have either a time-dependent anisotropy $r(t) = 0.29\exp(-t/33\text{ fs}) + 0.11$ (thin lines) or a constant r of 0.10 (thick line). Squares (□) show the raw anisotropy measured experimentally at 860 nm after broadband excitation. Insert: Calculated contributions from PFID, PPC, and GSB plus SE for the two-state system.

close to that of the complete calculation could be obtained by increasing the amplitude of the time-dependent term in $r(t)$ from 0.29 to 0.31 (not shown). Hence, part of the initial anisotropy estimated above from deconvolutions of the experimental data could reflect the neglect of PPC in the analysis.

Figure 6 also shows a similar calculation for the situation that the anisotropy decay comes entirely from pump−probe coherence coupling and PFID. The anisotropy of the SE plus GSB was taken to be 0.1, independent of time. The simulated anisotropy decayed from 0.4 to 0.1 very rapidly, essentially following the pump−probe cross correlation. The decay measured experimentally is significantly slower than this (see Figures 5 and 6). These simulations indicate that, although PPC probably increases the apparent values of $r(0)$, the measured

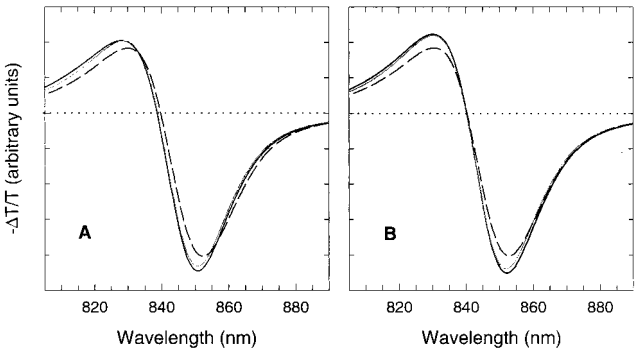

Figure 7. Calculated changes in isotropic absorption and stimulated emission caused by excitation of the B850 pigments with a pulse centered 184 cm^{-1} to the blue (A) or 222 cm^{-1} to the red (B) of the calculated absorption maximum. Results are shown for three idealized states of an ensemble with Gaussian disorder in the monomer transition energies ($\sigma = 200$ cm^{-1}): a coherent superposition of exciton states (solid black line), an incoherent mixture of exciton states with the same populations (gray line), and a Boltzmann equilibrium of exciton states at 295 K (dashed black line).

decay kinetics cannot be explained in this way and most likely are dominated by the actual dynamics of the system.

3. Theory. The spectroscopic relaxations described above can be explained by considering the exciton states of the LH2 complex. To simplify the model, we included only the Q_y transitions of the B850 BChls. GSB, SE, and ESA spectra were calculated for ensembles of complexes in which the monomer transition energies were normally distributed with a standard deviation σ of either 200 or 300 cm^{-1}. Previous work[4] has shown that the ground-state absorption and CD spectra can be described reasonably well by using $\sigma \approx 200$ cm^{-1}. With the present model and a homogeneous fwhm of 250 cm^{-1}, this value of σ gave a ground-state absorption spectrum that peaked at 848 nm and had a fwhm of 320 cm^{-1}. Except where stated, we will describe only the results obtained with these parameters.

The calculations were done for impulsive excitation on either the blue or red side of the absorption band and for three idealized states of the ensemble: (1) a coherent superposition of exciton states created at zero time, (2) an incoherent mixture of exciton states with the same populations, and (3) a Boltzmann equilibrium of exciton states within each LH2 complex at 295 K. Figure 7 shows the calculated isotropic signals for the three states. A comparison of the curves for cases 1 and 3 shows that relaxation from a coherent superposition of exciton states to a Boltzmann equilibrium would cause a red shift of the signals after blue excitation and mainly a decrease in amplitude after red excitation. The relative magnitudes of the calculated relaxations are similar to the magnitudes seen experimentally (Figure 2A,B), though somewhat smaller than those obtained by SVD of the experimental data (Figure 2C,D).

The calculated spectra for blue and red excitation remain slightly different following thermalization: the former is shifted

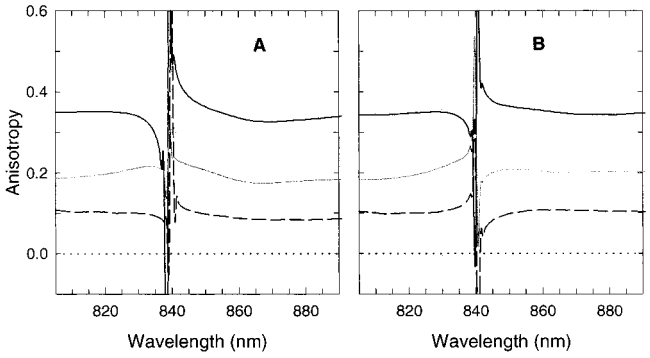

Figure 8. Calculated anisotropies of the changes in absorption and stimulated emission following blue (A) or red (B) excitation as in Figure 7. The line types correspond to those in Figure 7.

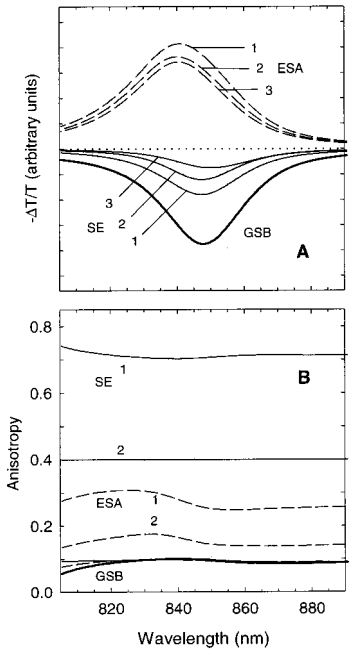

Figure 9. Isotropic amplitudes (A) and anisotropies (B) of the components of the calculated signals for blue excitation. Thin solid lines, stimulated emission; thick solid line, ground-state bleaching; dashed lines, excited-state absorption; 1, coherently excited ensemble; 2, incoherently excited ensemble; 3, thermalized ensemble. Dephasing and thermalization of the excited ensemble do not change the GSB. The dotted line in A is the zero of the ordinate scale.

to shorter wavelengths by about 1 nm. This is because the inhomogeneous distribution of monomer transition energies is considered to be static, and the model allows thermal equilibration of the exciton levels only within individual LH2 complexes (see Methods). Experimentally, although the excited states generated by blue or red excitation reached a quasiequilibrium within 350 fs, small differences remained for several ps (Figure 3). The decay of the residual differences could reflect energy transfer from one LH2 complex to another or slow fluctuations of the monomer energies within the complexes.

Figure 8 shows the calculated anisotropies for the three states. Perhaps surprisingly, the anisotropies are relatively insensitive to wavelength, except near the discontinuities where opposing contributions from ESA and GSB cause ($S_{\parallel} - S_{\perp}$) and ($S_{\parallel} + 2S_{\perp}$) to go through zero at slightly different wavelengths. In the regions where the signals are large, the initial anisotropy associated with a coherently excited ensemble is in the range of 0.35, and the final anisotropy after thermal equilibration is about 0.1. These values agree reasonably well with the experimental results obtained by excitation on the blue or red sides of the absorption band (Table 2), although the calculated anisotropies for the coherent excitation are somewhat smaller than the measured values of $r(0)$. Using a broad-band excitation pulse centered on the absorption maximum gave a calculated anisotropy for the coherent excitation that was higher by 0.014 at 860 nm and less sensitive to the probe wavelength. Increasing σ to 300 cm^{-1} decreased the anisotropy for the coherent excitation by 0.010 at 860 nm and increased the variation with wavelength.

Figure 9A shows the individual contributions of GSB, ESA, and SE to the calculated signals for blue excitation. Note first that the calculated SE is considerably weaker than the GSB. This is because the ground-state absorption represents the sum of the dipole strengths for 18 upward transitions, while emission represents the decay of a single excited state. SE decreases in amplitude as a result of electronic dephasing and then decreases further and shifts to longer wavelengths as a result of thermal equilibration with the weakly allowed states at low energies. Excited-state absorption also decreases, while GSB remains constant. Because of the opposing effects of ESA and SE, the loss of coherence causes relatively little change in the total signal (Figure 7); most of the relaxation of the total signal reflects the shift and decrease in SE that accompanies thermalization. This result depends to some extent on the assumed inhomogeneity of the ensemble. If the standard deviation of the monomer energies (σ) is increased to 300 cm^{-1}, electronic dephasing and thermalization contribute more equally to the spectral relaxation (not shown).

The calculated anisotropies of the GSB, ESA, and SE are plotted separately in Figure 9B. Stimulated emission from the coherently excited ensemble is calculated to have an anisotropy of approximately 0.71, with little dependence on wavelength. A value of 0.7 is expected for emission from a coherent superposition of two degenerate states with orthogonal transition dipoles,[18,29,30] and Kumble and Hochstrasser[31] have shown that if the excitation pulses were much broader than the B850 band one would always obtain a value of ~0.7 for the initial emission anisotropy regardless of the extent of inhomogeneous broadening. Contributions from out-of-plane transitions can lead to anisotropies exceeding 0.7.[18] Stimulated emission from the incoherently excited ensemble has the classical anisotropy of 0.4 expected for a single excited state with a fixed orientation, whereas the thermalized ensemble has the emission anisotropy of 0.1 expected for transition dipoles with random orientations in a plane. The calculated anisotropies for ESA depend more strongly on the wavelength, but are approximately 0.3, 0.15, and 0.1 for the coherent, incoherent, and thermalized excitations, respectively. GSB has an anisotropy of 0.1 over most of the B850 band, but becomes negative in the region of 780 nm where an out-of-plane exciton band contributes to the spectra.[3−6] Energy transfer among LH2 complexes with random orientations would reduce the anisotropies of SE, ESA, and GSB all to zero.

Discussion

The results presented in Figures 2 and 3 show that difference spectra created by excitation of B850 initially depend on the excitation wavelength, but relax to a quasiequilibrium with a time constant of 100 ± 20 fs. Excitation on the red side of the B850 band gives a somewhat shorter time constant than excitation on the blue side. A final equilibration occurs with a time constant of about 1 ps. Although the relaxation could have components with time constants of less than 50 fs, transients seen on this faster time scale are of questionable significance

because they probably include coherences between the pump and probe pulses. Our previous[17] estimate of 35 fs for the relaxation time constant reflected a larger contribution from these faster transients.

Excitation-dependent spectral relaxations of the LH2 complex have been described previously by Savikhin and Struve,[32] who identified a transient with a time constant of 80 to 100 fs at room temperature. In earlier one-color pump−probe experiments, Chachisvilis et al.[33] observed multiphasic relaxations of signals at 855, 864, and 882 nm. The major component had a time constant of about 60 fs at room temperature. The present measurements resolved the relaxation more clearly than was possible in the earlier work, but gave a similar time constant of 100 ± 20 fs.

In previous studies, Pullerits et al.,[19] Chachisvilis et al.,[33] and Jimenez et al.[34] have measured initial anisotropies between 0.3 and 0.4 and anisotropy decay times ranging from 40 to 200 fs. We found the signals to have an initial anisotropy in the range of 0.35−0.55, depending on the width of the excitation pulse. The anisotropy decayed to an asymptotic value close to 0.1 with a time constant on the order of 30 fs. When the LH2 complex was excited with a spectrally broad pulse, the anisotropies measured at wavelengths where ESA dominates were similar to the anisotropies at wavelengths where GSB and SE dominate (see Table 1). The initial anisotropy at 860 nm also was relatively insensitive to the excitation wavelength (Table 2), in spite of the fact that the relative contributions of ESA, GSB, and SE to the initial signal at 860 nm depend on the excitation (Figure 2). Narrowing the excitation pulse spectrum decreased the initial anisotropy at 860 nm to approximately 0.4 (compare Tables 1 and 2), possibly because it restricted the coherent excitation of nondegenerate states.

Several different processes could contribute to the spectral relaxations and the rapid decay of the anisotropy. These include (a) decay of electronic coherences within the manifold of exciton states, (b) thermal equilibration among excitonic states, (c) vibrational cooling and equilibration (Stokes shifts), (d) stochastic hopping of excitations localized on BChl dimers or other small clusters, and (e) energy transfer among separate LH2 complexes. A complete analysis of the dynamics of these processes is a challenging task because the LH2 complex has a large number of accessible excited states and because the interactions of the pigments with the protein probably fluctuate on many different time scales. However, Figures 7 and 8 show that the main features of the spectral relaxations and the decay of anisotropy are reproduced well by a model that considers only processes a and b. This conclusion is in accord with recent calculations by Kühn and Sundström[13] and Zhang et al,[14] who have used similar density-matrix formalisms to analyze the excited LH2 complex. Our calculations also are qualitatively consistent with the finding that the initial and final anisotropies are similar in regions where the signals are dominated by either ESA, GSB or SE. As suggested above, the small component of the relaxations with a time constant of about 1 ps could reflect thermalization of the monomer transition energies (processes c and d) or energy transfer from one LH2 complex to another (process e).

Kühn and Sundström[13] have calculated the dynamics of the relaxations by using multilevel Redfield theory with an explicit spectral density function. The predicted time scale of 0.5 to 1 ps is longer than the observed relaxation time of 0.1 ps, but seems reasonably close considering the complexity of the system. We have not attempted to calculate the dynamics theoretically in the present study. However, the model described above appears capable of rationalizing the observation that the anisotropy decay is faster than the spectral relaxations. With $\sigma = 200$ cm^{-1}, electronic dephasing causes a large decrease in the calculated anisotropy (Figure 8), whereas the relaxations of the overall signal occur mainly during thermalization (Figure 8). This is because the two most strongly allowed exciton states tend to be close together in energy[35] and to have approximately orthogonal transition dipoles; dephasing and equilibration of these states contributes strongly to the decay of the emission anisotropy, but has relatively little effect on the emission amplitude or wavelength. Dephasing is expected to occur rapidly as a result of both static inhomogeneity and fluctuations of the exciton energies, in addition to population decays.[35]

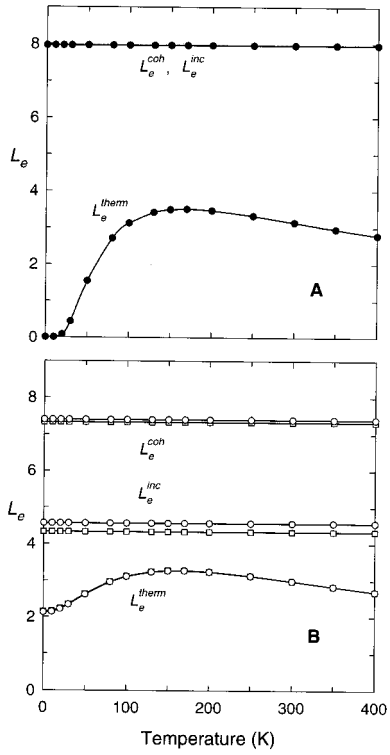

Figure 10. Calculated L_e^{coh}, L_e^{inc}, and L_e^{therm} (A) for a homogeneous ensemble of LH2 complexes ($\sigma = 0$) and (*B*) for an inhomogeneous ensemble ($\sigma = 200$) with blue (□) or red (○) excitation.

The calculated differences between the emission strengths of LH2 ensembles with coherent, incoherent, or thermalized excitations can be expressed conveniently by the function L_e as defined in eqs 8 and 9. L_e gives the isotropic emission strength, integrated over the emission spectrum, relative to the absorption strength of monomeric BChl in solution. It is similar to the "superradiance enhancement factor" (L_s) used by Mukamel and co-workers,[12,14] but is defined in an averaged exciton basis rather than the site (individual BChl) basis and includes an explicit dependence on the excitation pulse. Figure 10 shows the calculated L_e as a function of temperature for coherently excited, incoherently excited, and thermalized ensembles. Values are given for both homogeneous and inhomogeneous ensembles ($\sigma = 0$ or 200 cm^{-1}). With excitation pulses on either side of the absorption band, L_e for the coherently excited inhomogeneous ensemble (L_e^{coh}) is approximately 8. L_e decreases to about 4.5 as the excitation dephases (L_e^{inc}), and to approximately 3 after thermalization at 295 K (L_e^{therm}). L_e^{therm} increases slightly with decreasing temperature down to 150 K and then decreases to 2.1 at 0 K. The temperature dependence thus is relatively weak, in agreement with previous calculations by Zhang et al.[14] and with the fluorescence measurements described

by Monshouwer et al.[16] The calculated variation of L_e^{therm} with temperature is reduced further if the distribution of monomer transition energies is broadened by using $\sigma = 300$ cm^{-1} (not shown). In a homogeneous ensemble of LH2 complexes, L_e^{therm} drops almost to zero at low temperatures (Figure 10A).

The L_e^{therm} of 3 calculated for the inhomogeneous ensemble at 295 K agrees well with experimental measurements of the radiative rate constant.[16,36] L_e^{inc} and L_e^{therm} both would reduce to 1 if the electronic coupling between the BChls were removed. However, an L_e^{therm} of 3 does not imply that the excitation is localized on approximately three BChls, as has been suggested,[16,36] because the expected value of L_e^{therm} depends on the geometry of the complex. A homogeneous ensemble of LH2 complexes, in which the lowest exciton state is distributed almost uniformly around the ring and the two allowed states have approximately equal lobes of excitation density on opposite sides of the ring,[3,4] gives an L_e^{therm} that is only slightly larger than 3 at 295 K (Figure 10A).

At room temperature, L_e^{coh} and L_e^{inc} provide a clearer distinction between homogeneous and inhomogeneous ensembles. In the homogeneous ensemble L_e^{coh} is essentially the same as L_e^{inc}; in the inhomogeneous ensemble they differ by about a factor of 2 (see Figure 10). This is because the transition dipoles of the two allowed exciton transitions in a homogeneous ensemble are close to perpendicular, so that the terms $(\vec{\mu}_a \cdot \vec{\mu}_b)^2$ in eq 9a vanish except when $a = b$.

Previous workers have used a variety of other functions to describe the extent of exciton localization in the LH2 complex. Kühn and Sundström[13] used the function

$$c_n(t) = \sum_i |\langle \rho^s_{i,i+n}(t) \rangle_E| \qquad (14)$$

which expresses the average correlation between the excited-state wavefunctions of BChls i and $i + n$. Here $\boldsymbol{\rho}^s$ is the reduced density matrix in the site representation [$\rho^s_{i,i+n}(t) = \sum_a \sum_b C_i^a C_{i+n}^a \rho_{a,b}(t)$]. The coherent and thermalized excitations in our model give values of c_n similar to the values that Kühn and Sundström calculated for short and long times, respectively. Like L_e, c_n is a property of an ensemble. Even after thermalization, each individual complex still can be described well as being in an exciton state that is a property of the entire ring, although the electron distributions in these states vary from complex to complex.

The calculated spectra shown in Figures 7 and 9 differ from the measured spectra (Figures 2 and 3) in the breadth of the stimulated emission. The experimental spectra have a more pronounced tail at long wavelengths (see Figures 2 and 3). A comparison of the spectra calculated by Kühn and Sundström[13] with spectra measured by Chachisvilis et al.[33] shows a similar discrepancy (see Figure 2 in ref 13). The discrepancy also appears in the calculations by Alden et al.,[4] where the energy difference between the main absorption peak and the low-energy shoulder is about half the difference measured by hole burning.[9] The width of the calculated emission spectrum can be increased by broadening the distribution of monomer transition energies (with some degradation of the calculated anisotropies), or by using a larger homogeneous linewidth. Wu et al.[15] have shown that agreement between the calculated and observed ground-state spectra can be improved by introducing distortions with E_1 symmetry in place of the Gaussian disorder used here and by Alden et al. and Kühn and Sundström.

Discrepancies between the calculated and measured spectra of stimulated emission could arise from the neglect of vibrational relaxations in the calculations (process *c* above). However, hole-burning studies[9] indicate that electron−phonon coupling in the LH2 complex is relatively weak, which implies that vibrational contributions to the Stokes shift probably are small compared to electronic relaxations. In addition, observations of vibrational coherences persisting for several picoseconds[33] indicate that vibrational relaxations probably are unimportant on the short time scale probed in the present experiments.

Chachisvilis and Sundström[37] have shown that coherences between the ground state and doubly excited states can cause wavelength-dependent transients in the anisotropy signals if the transition dipoles for ground-state absorption and excited-state absorption are not parallel. Although coherences involving two-exciton states will need to be considered if the theoretical model used here is to be made more complete, our experimental results provide no clear evidence for such coherences because the initial anisotropy values are relatively insensitive to wavelength.

It is pertinent to ask whether the spectral relaxations could be explained as well by stochastic energy transfer between BChl dimers or other small clusters of pigments (process d above). In principle, absorption of light could generate localized excitations directly if the exciton coupling is less than the dispersion of the site energies or the homogeneous width of the absorption. The homogeneous width of the B850 transitions can be estimated from the values of T_2 obtained by fitting the PFID signals (Figure 4 and Table 1). Fits of the isotropic signals at 830, 850, or 860 nm following broad-band excitation gave $T_2 \approx 20$ fs, corresponding to a Lorentzian distribution with a fwhm of approximately 250 cm^{-1}. This is a maximum estimate of the homogeneous width because it neglects dephasing due to static inhomogeneity. From measurements of stimulated photon echoes, Jimenez et al.[38] have suggested that the homogeneous distribution is Gaussian and has a fwhm of 190 cm^{-1}. In the calculations shown in Figures 8−10 we used Lorentzian line shapes with a fwhm of 250 cm^{-1}. For comparison, the coupling strength between neighboring pigments is calculated to be on the order of 200 to 400 cm^{-1}.[3,4,39] The electronic coupling thus probably is at least as strong as the electron−phonon coupling, which means that the time constant for incoherent excitation transfer would be comparable to the coherence decay time. Energy transfer in B850 cannot, therefore, be truly incoherent. Still, to the extent that inhomogeneity of the monomer transition energies causes the exciton states to localize, fluctuations of these energies would result in stochastic hopping from one site to another, which could cause the spectroscopic properties to change with time.

Stochastic energy transfer would cause the GSB, SE, and ESA all to shift in the same direction. Excitation on the blue side of the band would be followed by spectral shifts to the red and vice versa. Although the observed signals do shift to longer wavelengths with time following blue excitation, excitation on the red side is followed by a decrease in amplitude throughout the spectrum but little or no shift (Figures 2 and 3). It is not clear how incoherent hopping of excitations among discrete sites could cause the signals to decrease in amplitude without shifting.[40] In principle, a red shift of the emission associated with vibrational relaxation could mask a blue shift associated with incoherent energy transfer. However, to account for the time-dependent decrease in the amplitudes of SE and ESA, we would have to postulate that the dipole strengths of the BChl dimers vary from site to site in a manner that correlates with the transition energies. This seems inconsistent with the observation that similar decreases in the signal amplitudes occur

when the system is excited on opposite sides of the B850 absorption band.

Conclusions

The shapes of the light-induced difference spectra measured immediately following excitation of B850 antenna complexes depend on the excitation wavelength, but the differences are mostly erased by a kinetic step with a time constant of 100 ± 20 fs. The signals have an initial anisotropy in the range 0.3−0.5, depending on the excitation pulse width; the anisotropy decreases to ~0.1 with a time constant of about 30 fs. The anisotropy is relatively independent of the excitation and detection wavelengths. Starting with the B850 pigments in the crystal structure of the LH2 antenna complex, we have calculated the ground-state absorption spectra for ensembles of LH2 complexes with Gaussian distributions of monomer transition energies, and have used a density-matrix treatment to calculate the light-induced changes in absorption and emission. Spectra were calculated for three idealized conditions: A coherent superposition of exciton states created by tunable broadband excitation, an incoherent mixture of exciton states with the same initial populations, and a Boltzmann distribution of exciton states within each complex. The calculated initial difference spectra depend markedly on the excitation wavelength, and the thermalized spectra less so, both in agreement with experimental results. The calculated anisotropies are comparatively insensitive to the excitation and detection wavelengths. The anisotropy decay is particularly sensitive to the loss of coherence, suggesting that the different time constants for the decay of anisotropy and spectral relaxation primarily reflect dephasing and thermalization, respectively.

Acknowledgment. We thank Rhett Alden for contributions to the exciton calculations, David Jonas for suggestions concerning anisotropy measurements, Oliver Kühn for helpful discussion of the relaxation dynamics, and Peter Schellenberg for a critical reading of the manuscript. This work was supported by the Chemical Sciences Division of the U.S. Department of Energy (Contracts FG06-94ER14443 and FG03-97ER14767) to V.N. and an NSF grant (Grant MCB-9111599) to W.P.

Appendix

The transition dipoles in eqs 1−6 are

$$\vec{\mu}_a = \sum_{i=1}^{N} C_i^a \, \vec{\mu}_i^m \tag{A1}$$

$$\vec{\mu}_{a\eta} = \sum_{j=1}^{N} \sum_{k_1=1}^{N} \sum_{k_2=k_1}^{N} C_j^a \, C_{k1,k2}^{\eta} \{\delta_{k1,k2}\delta_{j,k1}\phi\vec{\mu}_j^m + (1 - \delta_{k1,k2})(\delta_{j,k1}\vec{\mu}_{k2}^m + \delta_{j,k2}\vec{\mu}_{k1}^m)\} \tag{A2}$$

where $\vec{\mu}_i^m$ is the transition dipole of BChl monomer i, C_i^a is the coefficient for excitation of BChl i in one-exciton eigenstate a, C_{k_1,k_2}^{η} is the coefficient for excitation of BChls *k1* and *k2* in two-exciton eigenstate η, ϕ is the ratio of the magnitudes of the transition dipoles for the second and first excitations of an individual BChl, and the sums run over the 18 BChls.

The orientational averages are

$$\langle(\hat{x}\cdot\hat{\mu}_a)^2(\hat{x}\cdot\hat{\mu}_b)^2\rangle_O = (1 + 2\cos^2 \xi_a^b)/15 \tag{A3}$$

$$\langle(\hat{x}\cdot\hat{\mu}_a)^2(\hat{y}\cdot\hat{\mu}_b)^2\rangle_O = (2 - \cos^2 \xi_a^b)/15 \tag{A4}$$

$$\langle(\hat{x}\cdot\hat{\mu}_a)(\hat{x}\cdot\hat{\mu}_b)(\hat{y}\cdot\hat{\mu}_a)(\hat{y}\cdot\hat{\mu}_b)\rangle_O = (3\cos^2 \xi_a^b - 1)/30 \tag{A5}$$

$$\langle(\hat{x}\cdot\hat{\mu}_a)(\hat{x}\cdot\hat{\mu}_b)(\hat{x}\cdot\hat{\mu}_{a\eta})(\hat{x}\cdot\hat{\mu}_{b\eta})\rangle_O = \frac{1}{15}\{\cos \xi_a^b \cos \xi_{a\eta}^{b\eta} + \cos \xi_b^{b\eta} \cos \xi_a^{a\eta} + \cos \xi_a^{b\eta} \cos \xi_b^{a\eta}\} \tag{A6}$$

and

$$\langle(\hat{x}\cdot\hat{\mu}_a)(\hat{x}\cdot\hat{\mu}_b)(\hat{y}\cdot\hat{\mu}_{a\eta})(\hat{y}\cdot\hat{\mu}_{b\eta})\rangle_O = \frac{2}{15}\{\cos \xi_a^b \cos \xi_{a\eta}^{b\eta}\} - \frac{1}{30}\{\cos \xi_a^{a\eta} \cos \xi_b^{b\eta} + \cos \xi_a^{b\eta} \cos \xi_b^{a\eta}\} \tag{A7}$$

where ξ_a^b is the angle between $\hat{\mu}_a$ and $\hat{\mu}_b$.

References and Notes

(1) McDermott, G.; Prince, S. M.; Freer, A. A.; Hawthornthwaite-Lawless, A. M.; Papiz, M. Z.; Cogdell, R. J.; Isaacs, N. W. *Nature* **1995**, *374*, 517.
(2) Koepke, J.; Hu, X.; Muenke, C.; Schulten, K.; Michel, H. *Structure* **1996**, *4*, 581.
(3) Sauer, K.; Cogdell, R. J.; Prince, S. M.; Freer, A. A.; Isaacs, N. W.; Scheer, H. *Photochem. Photobiol.* **1996**, *64*, 564.
(4) Alden, R. G.; Johnson, E.; Nagarajan, V.; Parson, W. W.; Law, C. J.; Cogdell, R. J. *J. Phys. Chem. B* **1997**, *101*, 4667.
(5) Koolhaas, M. H. C.; van der Zwan, G.; Frese, R. N.; van Grondelle, R. *J. Phys. Chem. B* **1997**, *101*, 7262.
(6) Koolhaas, M. H. C.; Frese, R. N.; Fowler, G. J. S.; Bibby, T. S.; Georgakopoulou, S.; van der Zwan, G.; Hunter, C. N.; van Grondelle, R. *Biochemistry* **1998**, *37*, 4693.
(7) Fowler, G. J. S.; Visschers, R. W.; Grief, G. G.; van Grondelle, R.; Hunter, C. N. *Nature* **1992**, *355*, 848.
(8) Barkigia, K. M.; Chantranupong, L.; Smith, K. M.; Fajer, J. *J. Am. Chem. Soc.* **1988**, *110*, 7566. Prince, S. M.; Papiz, M. Z.; Freer, A. A.; McDermott, G. M.; Hathornthwaite-Lawless, A. M.; Cogdell, R. J.; Isaacs, N. W. *J. Mol. Biol.* **1997**, *268*, 412.
(9) Reddy, N. R. S.; Picorel, R.; Small, G. J. *J. Phys. Chem.* **1992**, *96*, 6458.
(10) Leegwater, J. A. *J. Phys. Chem.* **1996**, *100*, 14403.
(11) Kumble, R.; Palese, S.; Visschers, R. W.; Dutton, P. L.; Hochstrasser, R. M. *Chem. Phys. Lett.* **1996**, *261*, 396.
(12) Meier, T.; Chernyak, V.; Mukamel, S. *J. Phys. Chem. B* **1997**, *101*, 7332.
(13) Kühn, O.; Sundström, V. *J. Chem. Phys.* **1997**, *107*, 4154.
(14) Zhang, W. M; Meier, T.; Chernyak, V.; Mukamel, S. *J. Chem. Phys.* **1998**, *108*, 7763.
(15) Wu, H. M.; Ratsep, M.; Lee, I. J.; Cogdell, R. J.; Small, R. J. *J. Phys. Chem. B* **1997**, *101*, 7654.
(16) Monshouwer, R.; Abrahamson, M.; van Mourik, F.; van Grondelle, R. *J. Phys. Chem. B* **1997**, *101*, 7241.
(17) Nagarajan, V.; Alden, R. G.; Williams, J. C.; Parson, W. W. *Proc. Natl. Acad. Sci. U.S.A.* **1996**, *93*, 13774.
(18) van Amerongen, H.; Struve, W. S. *Methods Enzymol.* **1995**, *246*, 259.
(19) Pullertis, T.; Chachisvilis, M.; Sundström, V. *J. Phys. Chem.* **1996**, *100*, 10787.
(20) Becker, M.; Nagarajan, V.; Parson, W. W. *J. Am. Chem. Soc.* **1991**, *113*, 6840.
(21) Rahman, T. S.; Knox, R. S.; Kenkre, V. M. *Chem. Phys.* **1979**, *44*, 197.
(22) Chang, Y. J.; Cong, A. P.; Simon, J. D. *J. Chem. Phys.* **1997**, *106*, 8639.
(23) Brito Cruz, C. H.; Gordon, J. P.; Becker, P. C.; Fork, R. L.; Shank, C. V. *IEEE J. Quantum Electron.* **1988**, *24*, 261.
(24) Vos, M. H.; Breton, J.; Martin, J.-L. *J. Phys. Chem B.* **1997**, *101*, 9820.
(25) Yariv, A. *Quantum Electronics*, 3rd ed.; John Wiley & Sons, Inc.: New York, 1988 (Appendix 4).
(26) Pollard, W. T.; Mathies, R. A. *Ann. Rev. Phys. Chem.* **1992**, *43*, 497.
(27) Mukamel, S. *Principles of Nonlinear Optical Spectroscopy*; Oxford University Press: New York, 1994; Chapters 8, 11.
(28) Gottfried, D. S.; Stocker, J. W.; Boxer, S. G. *Biochim. Biophys. Acta* **1991**, *1059*, 63.
(29) Knox, R. S.; Gulen, D. *Photochem. Photobiol.* **1993**, *57*, 40.
(30) Wynne, K.; Hochstrasser, R. M. *J. Chem. Phys.* **1993**, *171*, 179.
(31) Kumble, R.; Hochstrasser, R. M. *J. Chem. Phys.* **1998**, *109*, 855.
(32) Savikhin, S.; Struve, W. S. *Chem. Phys.* **1996**, *210*, 91.

(33) Chachisvilis, M.; Kühn, O.; Pullerits, T.; Sundström, V. *J. Phys. Chem. B* **1997**, *101*, 7275.

(34) Jimenez, R.; Dikshit, S. N.; Bradforth, S. E.; Fleming, G. R. *J. Phys. Chem.* **1996**, *100*, 6825.

(35) In the inhomogeneous ensemble with $\sigma = 200$ cm^{-1}, the distribution $G(\Delta E_{ab})$ of the absolute value of the energy difference between the two most strongly allowed transitions (*a* and *b*) peaks at approximately 55 cm^{-1} and has a fwhm of 90 cm^{-1}. (Exciton interactions narrow the distribution of allowed excited states relative to the dispersion of the monomer transition energies.) The magnitude of the Fourier transform of $G(\Delta E_{ab})$ decreases to half its maximum value in 160 fs. The static inhomogeneity assumed in our LH2 model thus would cause the off-diagonal terms ρ_{ab} and ρ_{ba} of the density matrix to decay with a time constant on the order of 160 fs. This suggests that the more rapid dephasing indicated by the anisotropy decay ($\tau \approx 30$ fs) is driven mainly by dynamic processes that contribute to the homogeneous linewidth, such as population relaxations and rapid modulation of the state energies by interactions with the medium. Note that $G(\Delta E_{ab})$ here is for the energy difference between two exciton states, whereas the coupling strengths in eq 13 concern the distribution of energy difference between ground and excited states in a two-state model. The value of Δ_2 used in eq 13 (140 cm^{-1}) corresponds to an inhomogeneous fwhm of 330 cm^{-1}. The dephasing resulting from this inhomogeneity makes the dominant contribution to the rapid decay of the calculated PFID signal (see the insert in Figure 6).

(36) Leupold, D.; Stiel, H.; Teuchner, K.; Nowak, F.; Sander, W.; Ücker, B.; Scheer, H. *Phys. Rev. Lett.* **1996**, *77*, 4675.

(37) Chachisvilis, M.; Sundström, V. *J. Chem. Phys.* **1996**, *104*, 5734.

(38) Jimenez, R.; van Mourik, F.; Yu, J. Y.; Fleming, G. R. *J. Phys. Chem. B* **1997**, *101*, 7350.

(39) Krueger, B. P.; Scholes, G. D.; Fleming, G. R. *J. Phys. Chem. B* **1998**, *102*, 5378.

(40) To examine this point, we simulated excitation hopping in a model that included six absorbers with shifted Gaussian spectra. The centers of the individual absorption bands were distributed so that the spectrum of the collective system had a fwhm 1.5 times the fwhm of the spectrum of a single absorber (δ). The Stokes shift (2λ) for an individual absorber was related to δ by $2\lambda = \delta^2/(8k_BT \ln 2)$. No spatial arrangement was introduced in the model. The microscopic rate constant for excitation transfer from a given donor to an acceptor absorbing at lower energy was taken to be proportional to the overlap of the Stokes-shifted emission spectrum of the donor with the absorption spectrum of the acceptor; the rate constant for transfer in the opposite direction was reduced by the Boltzmann factor. The 6×6 rate matrix was diagonalized for a given initial distribution of excitations among the absorbers, and the eigenvalues were used to calculate the distribution of excitations as a function of time.[41] Absorption spectra of the ensemble then were calculated for various delay times and were analyzed by the same methods as used above for the experimental spectra. The relaxations were found to be biphasic, with time constants that were about 10 and 40 times the microscopic time constant for the fastest hop. Excitation anywhere in the inhomogeneous absorption band produced the same relaxation time constants. As expected, any change in the peak amplitude was always accompanied by a spectral shift.

(41) Steinfeld, J. I.; Fransisco, J. S.; Hase, W. L. *Chemical Kinetics and Dynamics*; Prentice-Hall: New Jersey, 1989.